

## Effect of Heat Input on Microstructure and Corrosion Behavior of High Strength Low Alloy Steel Welds

Hua Qin<sup>1,\*</sup>, Yingchun Tang<sup>2</sup>, Ping Liang<sup>1</sup>

<sup>1</sup> School of mechanical engineering, Liaoning Shihua University, Fushun 113001, China;

<sup>2</sup> Sino- German Institute of Shengyang Polytechnic College, Shenyang 110045, China.

\*E-mail: [huaq2008@163.com](mailto:huaq2008@163.com)

Received: 14 November 2020 / Accepted: 12 January 2021 / Published: 28 February 2021

---

High strength low alloy (HSLA) steel was welded by metal active gas arc welding (MAG), and the effect of heat input on microstructure and corrosion behavior of HSLA welds was investigated by optical microscope (OM), scanning electron microscopy (SEM), potentiodynamic polarization curves, electrochemical impedance spectroscopy (EIS) in this study. Results indicated that the volume percent of acicular ferrite (AF) in the weld increases first and then decreases with the increase of heat input, when the heat input is  $11.9\text{kJ}\cdot\text{cm}^{-1}$ , the proportion of acicular ferrite obtained in the weld reaches the maximum value. It is found that the type of microstructure has significant effect on corrosion behavior of the weld metal, the increase in the amount of acicular ferrite can result in corrosion property of the weld metal becoming worse in 3.5wt% NaCl solution. Moreover, the thickness and density of corrosion product on the surface of samples play a very important role in the corrosion behavior of the weld metal. When the corrosion product is loose, porous and defective, it provides minor protection for the weld metal, in this case, corrosion rate of the weld metal increases.

---

**Keywords:** HSLA steel; Heat input; Weld metal; Microstructure; Corrosion behavior

### 1. INTRODUCTION

High strength low alloy (HSLA) steel that usually serves as bridges, oil pipelines, hydropower and ocean engineering exhibits a good combination of mechanical performance and weldability [1]. Due to the high strength, the self-weight of welding structure can be reduced to achieve the purpose of saving steel. It has always attracted much attention from the engineering field and has been widely used in welding engineering structures for its significant economic benefits. When acicular ferrite (AF) is present in the weld metal of HSLA steel, the weld joint has better mechanical properties [2-4]. Because acicular ferrite exhibits higher strength and better toughness, it is hoped that acicular ferrite can appear in the weld metal during welding. When the weld metal composition and cooling conditions are

appropriate, the austenite can transform into acicular ferrite [5, 6]. Although the transition temperature range of acicular ferrite is similar to bainite, its microstructure and properties are different from bainite [7, 8]. In recent years, researchers have studied the nucleation, growth mechanism and characteristics of acicular ferrite, and some research results have been made in the acicular ferrite microstructure and mechanical properties, but limited investigations are focused on the effect of acicular ferrite on the weld metal corrosion behavior of HSLA steel [9, 10].

When both the welding wire and the base material are selected, microstructure and properties of the weld metal can be determined by the welding process conditions. The heat input in the welding process is a comprehensive parameter, it reflects the value of welding current, arc voltage and welding speed [11-13]. In this study, HQ100 steel welds was prepared by using metal active gas arc welding (MAG) under different heat input conditions. Furthermore, the effect of heat input on microstructure and corrosion behavior of the weld metal in 3.5wt% NaCl solution was investigated by optical microscope (OM), scanning electron microscopy (SEM), potentiodynamic polarization curves, electrochemical impedance spectroscopy (EIS).

## 2. EXPERIMENTAL

### 2.1 Materials

The composition of HQ100 steel and JM100 welding wire investigated in this work is given in Table 1 and Table 2, and the tensile strength of them is 1036 MPa and 715 MPa, respectively. The experimental steel were machined into 260 mm×150 mm×10 mm to prepare for welding.

**Table 1.** Chemical composition of HQ100 steel

C	Mn	P	S	Si	Cu	Cr
< 0.18%	0.6-1.2%	< 0.03%	< 0.03%	0.18-0.35%	0.15-0.5%	0.4-0.8%
Mo	V	Ni	Fe			
0.3-0.6%	≤0.1%	0.7-1.5%	Bal.			

**Table 2.** Chemical composition of JM100 welding wire

C	Mn	P	S	Si	Cr	Al	Ti
< 0.07%	1.61%	< 0.002%	< 0.002%	0.58%	0.4-0.8%	0.02%	0.092%
Mo	Ni	Fe					
0.39%	0.84%	Bal.					

## 2.2 Welding process

The experimental steel used for welding was in the form of butt with V shaped groove, and the angle of the groove was 60°, the blunt side and gap were both 2mm. YD-S00GL3 all-digital pulse welding machine was used to weld without preheating by MAG. Before welding, the groove was polished with grinding wheel to remove oil and oxide scales to avoid inclusions in the weld. 80% Ar + 20% CO<sub>2</sub> mixed gas was used as welding shielding gas, and gas flow rate was controlled at 16-17L · min<sup>-1</sup> during welding. The heat input was adjusted by changing the welding current and arc voltage, the welding parameters were presented in Table 3.

**Table 3.** Welding process parameters

Serial number	Welding current (I/A)	Arc voltage (U/V)	Welding speed (v/mm·s <sup>-1</sup> )	Heat input (q/kJ·cm <sup>-1</sup> )
1	240	25-26	5.4	9.2
2	260	27.2-27.6	5.4	10.7
3	270	29.5-30.0	5.4	11.9
4	280	31.3-32.1	5.4	13.0
5	290	33.5-34.0	5.4	14.4
6	310	35.2-36.5	5.4	15.9

## 2.3 Microstructure observation

For optical observation, the weld metal sample was ground and mechanically polished, subsequently, it was etched with 4% (volume fraction) nitric alcohol solution. Optical microscopy (OM, Leica Qwin500) and scanning electron microscopy (SEM, TESCAN VEGA3) with energy dispersive spectrum (EDS) were used for observation and analysis microstructure of the weld metal under different heat input.

## 2.4 Corrosion test

Weight loss and depth tests were conducted to measure the corrosion rate of the weld metal. The samples under different heat input were washed, dried and weighed. The tests were performed in 3.5wt% NaCl solution at temperature of 20°C for 10 days. Three equivalent samples were used for each heat input condition to ensure experimental reproducibility. The corrosion surface morphology of the weld metal was characterized using SEM. The samples after corrosion were rinsed with rust removal solution (50 mL hydrochloric acid + 6 g hexamethylenetetramine + 50 mL deionized water) for 3-5 min., and then dried again. The weight loss can be calculated as:

$$v_1 = \frac{w_0 - w_1}{s \times t}, \text{ (g/m}^2 \cdot \text{h)} \quad (1)$$

$$v_2 = \frac{v_1 \times 8.75}{\rho}, \text{ (mm/a)} \quad (2)$$

Where  $v_I$  is the corrosion rate,  $w_0$  and  $w_I$  are the original and final weight of sample, respectively,  $s$  is the exposed surface area of sample,  $t$  is the corrosion time, and  $\rho$  presents the density.

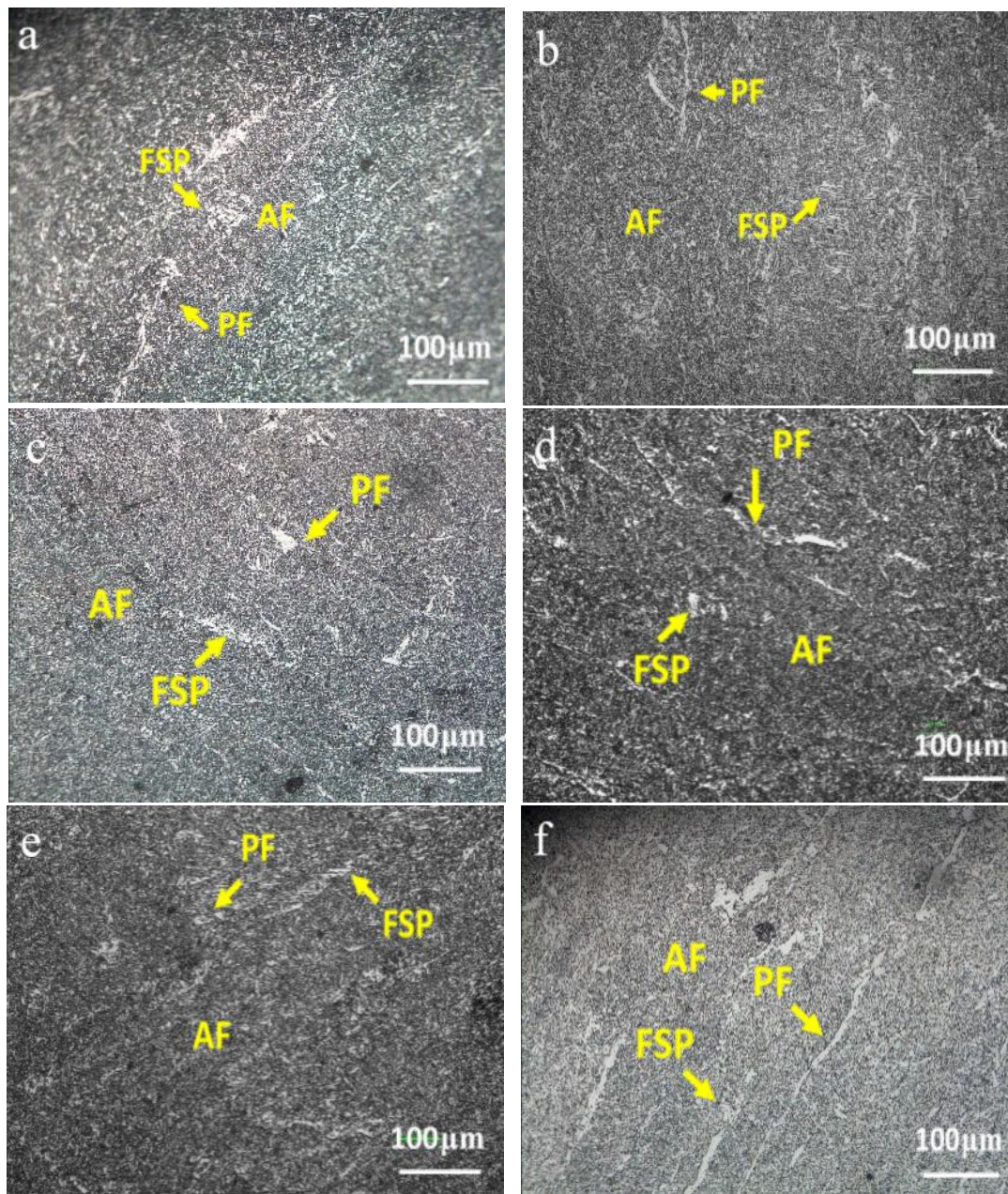
Electrochemical measurements were performed with a three-electrode to use PARSTAT2273 advanced electrochemical workstation. The weld metal sample embedded in PVC pipe using epoxy resin with an exposed area was used as the working electrode (WE). Saturated calomel electrode (SCE) and graphite were used as reference electrode (RE) and counter electrode (CE), respectively. After the open circuit potential (OCP) of the samples was stabilized, the potentiodynamic polarization and impedance curve for the weld were measured under different heat input. Under each condition, three measurements were conducted to confirmed the reliability of results.

Before the electrochemical measurements, the working surfaces were grounded with water proof papers up to 1000 mesh, and the samples were washed with deionized water. Moreover, in order to obtain corrosion products, the samples were immersed in 3.5wt% NaCl solution for 5 days and 11 days, respectively. The samples with corrosion product were carried out polarization and impedance test. The potentiodynamic polarization was applied by sweeping the potential in the positive direction at 1mV/s from -0.3 V to 1.3 V, and electrochemical impedance spectroscopy (EIS) was performed by 10 mV amplitude sinusoidal voltage as the disturbance signal for frequencies ranging from  $10^5$  Hz to 1 Hz at OCP. The electrode area of samples is 1 cm<sup>2</sup>, and all experiments were performed at room temperature.

### 3. RESULTS AND ANALYSIS

#### 3.1 Microstructural observation

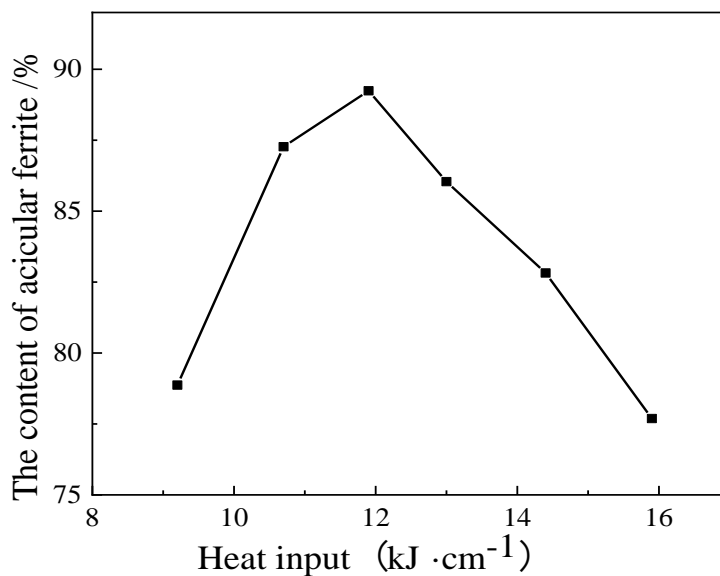
Optical micrographs of the samples at different heat input present in Fig. 1. It can be seen that microstructure of the weld metal is composed of polygonal ferrite (PF) distributed along the grain boundary, the ferrite side-plate (FSP) growing from grain boundary into grain and acicular ferrite (AF) interlocked growth in intergranular. When the weld metal is cooled to a higher temperature (770 °C-680 °C), the grain boundary has higher energy, it can provide nucleation conditions for the formation of PF, PF is preferentially formed at the prior austenite grain boundaries, and it is distributed along the grain boundaries, which are characterized in strips or polygons. The weld metal stays longer at high temperature or cools down more slowly, and the amount of PF in the weld metal can significantly increases [14,15]. The temperature of FSP formation is lower than that of PF, and the slatted or jagged ferrite is clearly visible in the weld metal [16, 17]. The AF is acicularly distributed in the prior austenite grains, it can grow radially with micro-inclusions as the core, such as oxides and nitrides [18].



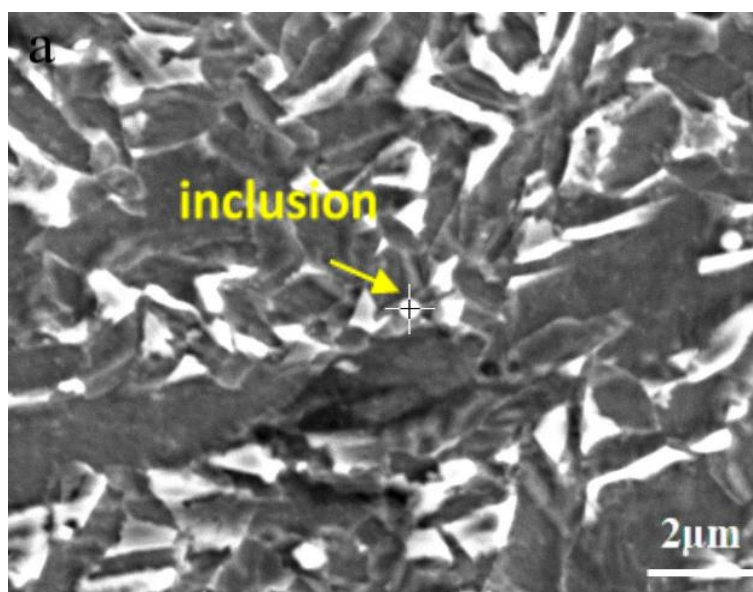
**Figure 1.** Microstructure of the weld metal at different heat input conditions for HQ100 steel: (a) 9.2  $\text{kJ} \cdot \text{cm}^{-1}$ , (b) 10.7  $\text{kJ} \cdot \text{cm}^{-1}$ , (c) 11.9  $\text{kJ} \cdot \text{cm}^{-1}$ , (d) 13.0  $\text{kJ} \cdot \text{cm}^{-1}$ , (e) 14.4  $\text{kJ} \cdot \text{cm}^{-1}$  and (f) 15.9  $\text{kJ} \cdot \text{cm}^{-1}$ .

The JM100 welding wire was used to weld experimental steel under different heat input, the volume percent of AF in the weld metal can also be different, as shown in Fig. 2. For the heat input of  $9.2 \text{ kJ} \cdot \text{cm}^{-1}$ , the amount of AF is 78.87%. As the heat input is increased to  $10.7 \text{ kJ} \cdot \text{cm}^{-1}$  and  $11.9 \text{ kJ} \cdot \text{cm}^{-1}$ , the amount of AF is 87.27% and 89.24%, respectively. Subsequently, as the heat input is further increased, the amount of AF in the weld metal decreases. This shows that under both low and high heat input, the amount of AF in weld metal can decrease. When the heat input is lower or the cooling rate is faster, AF does not have enough time to nucleate and grow on the micro-inclusions, and phase

transformation carries out insufficiently, which can cause reduction in the amount of AF in the weld metal. Conversely, when the heat input is higher and the cooling rate is slower, the weld metal stays at high temperature for long time, which is more conducive to the formation of PF and FSP, and the amount of AF in the weld metal also reduces.



**Figure 2.** The volume percent of acicular ferrite in weld metal at different heat input 9.2 kJ · cm<sup>-1</sup>, 10.7 kJ · cm<sup>-1</sup>, 11.9 kJ · cm<sup>-1</sup>, 13.0 kJ · cm<sup>-1</sup>, 14.4 kJ · cm<sup>-1</sup> and 15.9 kJ · cm<sup>-1</sup>



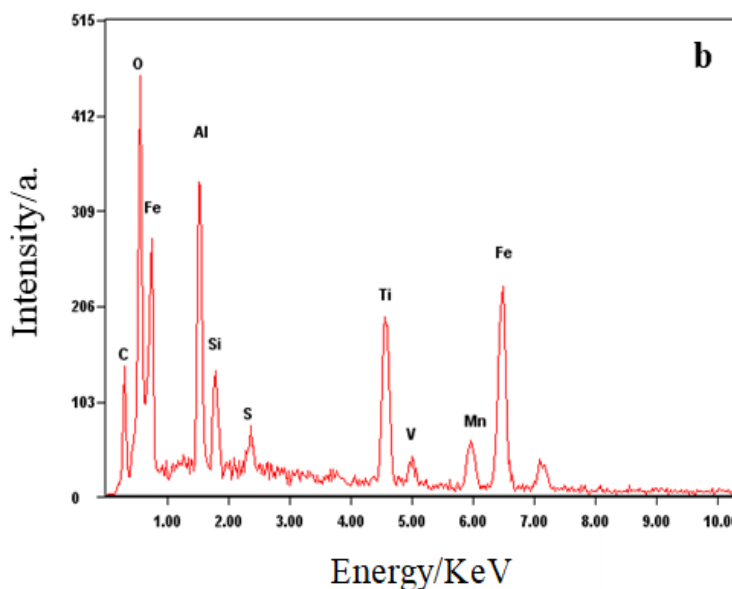


**Figure 3.** SEM photo (a) and EDS spectrum (b) of micro-inclusion in the weld metal of HQ100 Steel

As observed in Fig. 3, the micro-inclusions in weld metal contain some elements such as Ti, Si, Al, Mn, V, S and O by energy dispersive spectrum analysis. Because the local area of the micro-inclusion surface has higher surface energy, it can facilitate the non-uniform nucleation of AF, and the oxides and sulfides or complexes formed by these elements can induce AF nucleation on the surface of micro-inclusions [19, 20]. If the micro-inclusion has a higher melting point, it has a higher surface energy. For example, TiO<sub>2</sub>, Al<sub>2</sub>O<sub>3</sub>, MnO, SiO<sub>2</sub>, MnS have high surface energy, they can provide favorable conditions for acicular ferrite nucleation, which is conducive to AF nucleation at grain boundaries or intragranular [20-23].

### 3.2 Corrosion rate test

**Table 4.** Corrosion rate of the weld metal under different heat input in 3.5wt% NaCl solution for 10 days

Heat input (kJ·cm <sup>-1</sup> )	Initial weight (g)	final weight (g)	Sample size (mm)	Corrosion rate (g/m <sup>2</sup> ·h)	Corrosion depth (mm/a)
9.2	1.3469	1.34	10×10×2	0.1027	0.114
10.7	1.3476	1.3355	10×10×2	0.1801	0.201
11.9	1.2258	1.2119	10×10×2	0.2068	0.231
13.0	0.3172	0.313	6×5×2	0.1482	0.165
14.4	1.1386	1.1317	10×10×2	0.1027	0.114
15.9	0.9766	0.9708	7×10×2	0.1162	0.129

The corrosion rates of the weld metal in 3.5wt% NaCl solution for 10 days, calculated from the

weight loss tests, are listed in Table 4. The corrosion rates of the weld metal under different heat input conditions are on the same order of magnitude. As observed in Table 4, both the corrosion rate and corrosion depth show a trend of first increase and then decrease with the increase of heat input. When the heat input amounts to  $11.9 \text{ kJ} \cdot \text{cm}^{-1}$ , the corrosion rate and corrosion depth of the weld metal reach the maximum value, and corrosion property of the weld metal become worse.

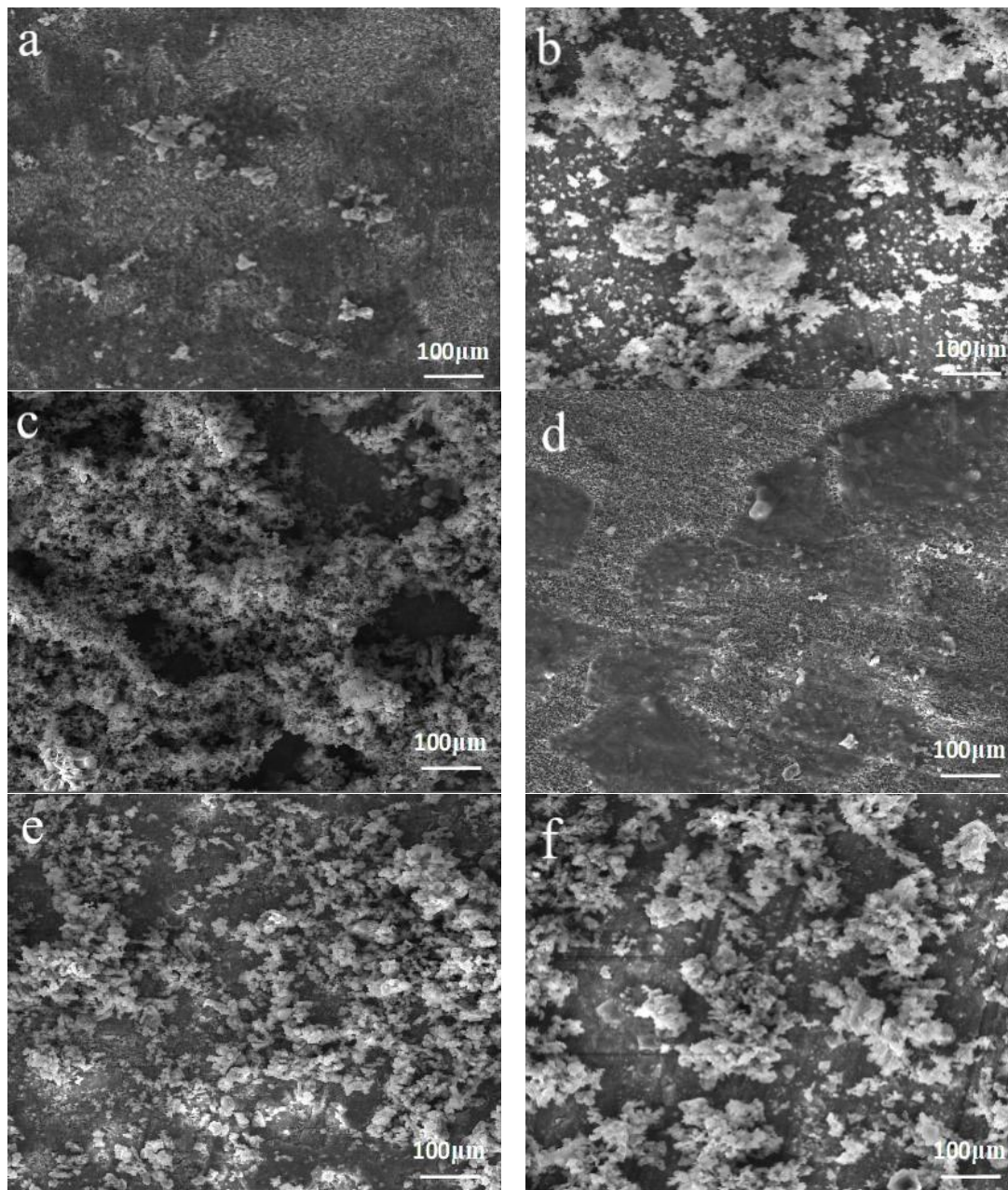


**Figure 4.** Surface morphology of the weld after soaking in 3.5wt% NaCl solution for 10 days under different heat input conditions (a:  $9.2 \text{ kJ} \cdot \text{cm}^{-1}$ , b:  $10.7 \text{ kJ} \cdot \text{cm}^{-1}$ , c:  $11.9 \text{ kJ} \cdot \text{cm}^{-1}$ , d:  $13.0 \text{ kJ} \cdot \text{cm}^{-1}$ , e:  $14.4 \text{ kJ} \cdot \text{cm}^{-1}$  and f:  $15.9 \text{ kJ} \cdot \text{cm}^{-1}$ ).

Under different heat input conditions, the surfaces of the weld metal were macroscopically

observed after immersing in 3.5wt% NaCl solution for 10 days. It can be seen that the surfaces of the samples are covered by a yellow-brown corrosion products, and the corrosion products are unevenly distributed on the surface of the weld metal.

Corrosion product morphologies of samples are presented in Fig. 4, when the heat input is 9.2  $\text{kJ} \cdot \text{cm}^{-1}$  and 15.9  $\text{kJ} \cdot \text{cm}^{-1}$ , the corrosion product is relatively uniform by Fig. 4a and Fig. 4f. In the case of other heat input, it can be seen that NaCl crystallizes at local locations on the surface of samples, which can cause uneven corrosion on the surface of the weld metal, and the samples exhibit localized corrosion behavior, as shown in Fig. 4(b-e).

### 3.3 Electrochemical corrosion behavior

Polarization curve and electrochemical impedance spectroscopy(EIS) of the weld metal under different heat input in 3.5wt% NaCl solution are presented in Fig. 5a and Fig. 5b, and electrochemical equivalent circuit for fitting impedance spectrum data of the weld metal is R[QR]. The fitted electrochemical corrosion parameters, such as corrosion potential ( $E_{\text{corr}}$ ), self-corrosion current ( $I_{\text{corr}}$ ), solution resistance ( $R_s$ ) and charge transfer resistance ( $R_{\text{ct}}$ ), are shown in Table 5. The weld metal samples under different heat input have similar polarization behavior in 3.5wt% NaCl solution by Fig. 5a, it indicates that the weld metal can occur electrochemical corrosion behavior in 3.5wt% NaCl solution. The metal dissolves at the anode, and the cathode is controlled by the oxygen depolarization process [24,25]. With the increase of heat input,  $I_{\text{corr}}$  shows the change of first increasing and then decreasing. According to Faraday's second law, there is a proportional relationship between the corrosion current density and the corrosion rate [26]. The greater corrosion current is, the faster metal corrosion rate is. When the heat input is 11.9  $\text{kJ} \cdot \text{cm}^{-1}$ ,  $I_{\text{corr}}$  is 24.38  $\mu\text{A} \cdot \text{cm}^{-2}$ , and the corrosion rate is the largest.

As observed in Fig. 5b, when the heat input is 10.7  $\text{kJ} \cdot \text{cm}^{-1}$ , capacitive semicircle reaches the lowest, and the sample corrosion rate is the highest, it indicate that corrosion property of the weld metal becomes to deteriorate.

**Table 5.** Electrochemical test parameters of the weld metal under different heat input in a 3.5wt% NaCl solution

Heat input ( $\text{kJ} \cdot \text{cm}^{-1}$ )	$E_{\text{corr}}$ (mV)	$I_{\text{corr}}$ ( $\mu\text{A} \cdot \text{cm}^{-2}$ )	$R_s$ ( $\Omega \cdot \text{cm}^2$ )	$R_{\text{ct}}$ ( $\Omega \cdot \text{cm}^2$ )
9.2	-612	12.15	7.67	796
10.7	-730	23.78	5.95	245
11.9	-578	24.38	4.45	475
13.0	-591	16.82	5.35	497
14.4	-606	12.90	6.61	728
15.9	-608	12.22	7.64	974

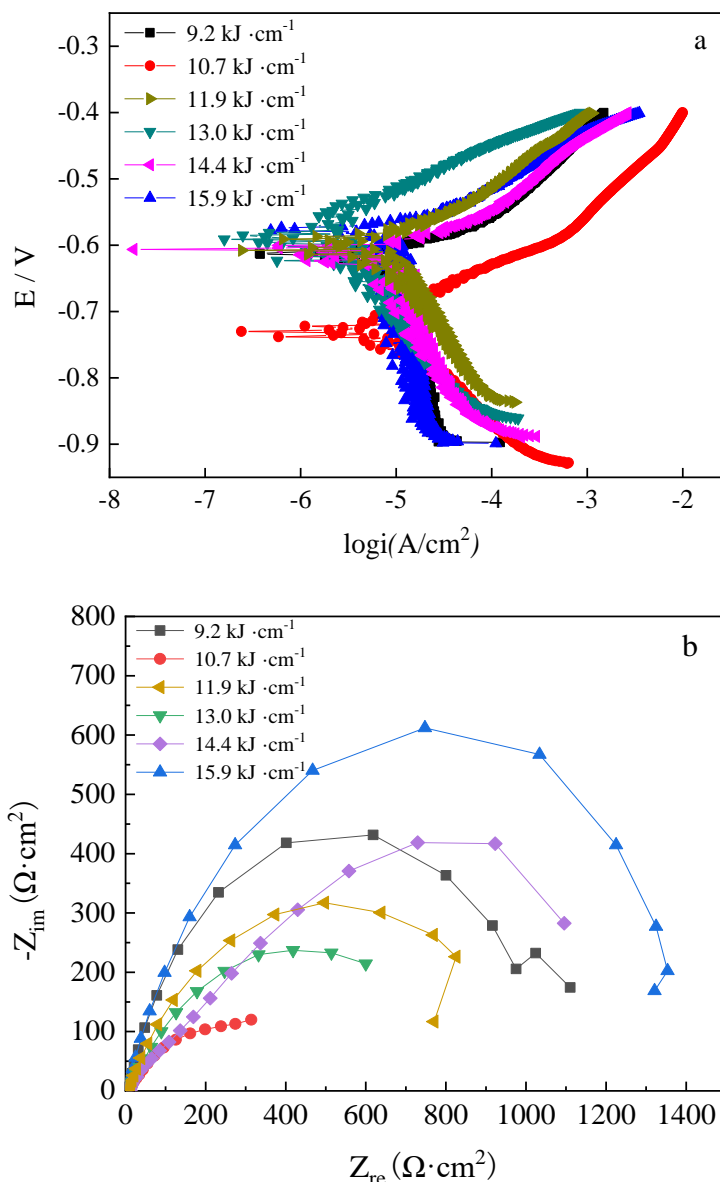


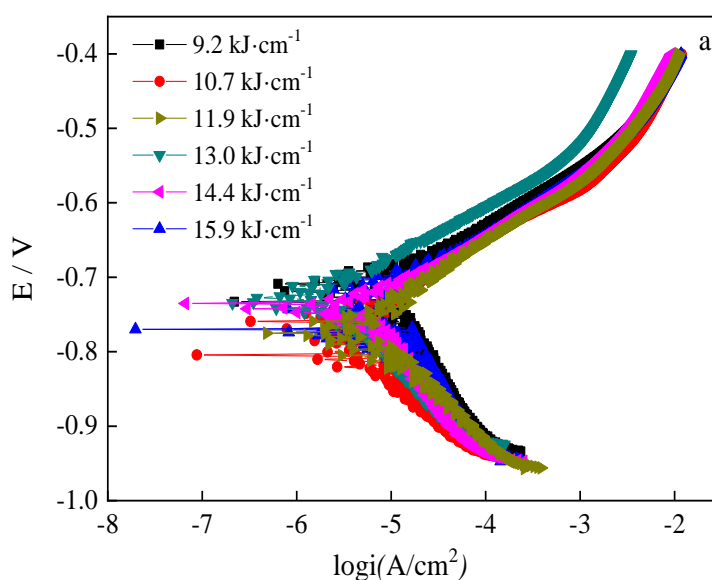
**Figure 5.** Electrochemical corrosion behavior of the weld under different heat input 9.2  $\text{kJ} \cdot \text{cm}^{-1}$ , 10.7  $\text{kJ} \cdot \text{cm}^{-1}$ , 11.9  $\text{kJ} \cdot \text{cm}^{-1}$ , 13.0  $\text{kJ} \cdot \text{cm}^{-1}$ , 14.4  $\text{kJ} \cdot \text{cm}^{-1}$  and 15.9  $\text{kJ} \cdot \text{cm}^{-1}$  in 3.5wt% NaCl solution (a: Potential polarization curve and b: EIS)

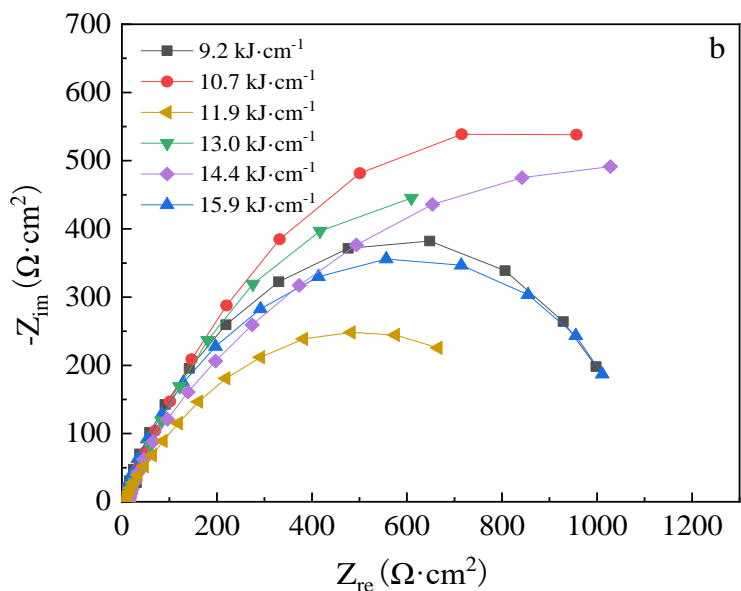
The weld metal samples under different heat input conditions were immersed in 3.5wt% NaCl solution for 5 days and 11 days, respectively, and the samples with corrosion products were subjected to electrochemical polarization and impedance test. The influence of corrosion products on the electrochemical corrosion behavior of the weld metal in 3.5% NaCl solution is analyzed by Fig. 6 and Fig. 7. The equivalent circuit of fitting impedance spectrum data is  $R[QRQR]$ , as shown in Fig. 8. In this circuit,  $R_s$  represents the solution resistance,  $R_f$  is the film resistance due to the formation of corrosion products, while  $R_{ct}$  means the charge transfer resistance,  $CPE_1$  is the constant phase element of corrosion products layer, and  $CPE_2$  presents the constant phase element of the weld metal surface. The shape of the polarization curve of the samples with corrosion products is well-defined, and they have a common

feature for measured plots. It is shown that the existence of the film only affects the current of the cathode and anode reactions, it does not change the anode and cathode reaction mechanism of the weld metal in the electrolytic solution.

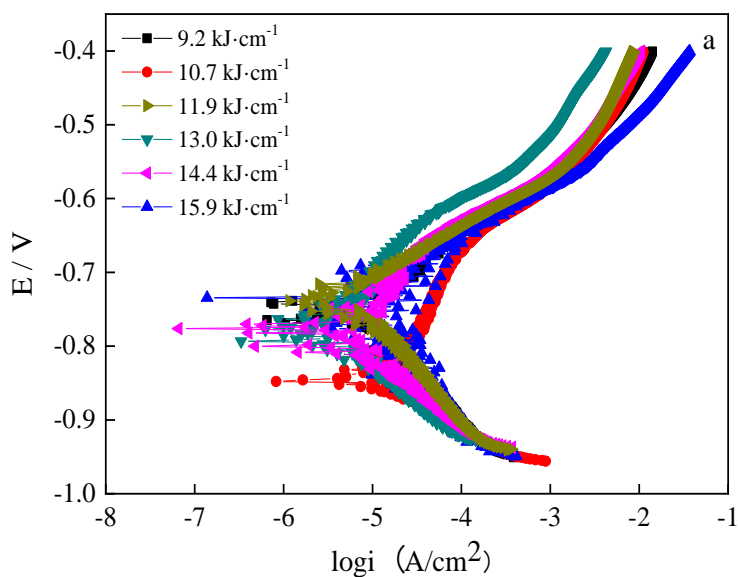
After the weld metal is immersed in 3.5% NaCl solution for 5 days, dense corrosion product film have formed on the surface of the samples. The electrochemical fitting data is compared with Table 5, it can be seen that  $I_{corr}$  of the weld metal significantly decreases under different heat input. The film acts as an electrode to cause an electrochemical reaction, it can protect the weld metal and slow down the corrosion rate of the weld metal. When the heat input is  $10.7 \text{kJ} \cdot \text{cm}^{-1}$ ,  $I_{corr}$  of the weld metal is  $5.08 \mu\text{A} \cdot \text{cm}^{-2}$ , and  $R_f$  is  $1499 \Omega \cdot \text{cm}^2$ . Compared without corrosion product on the surface of samples, the corrosion product can increase the charge transfer resistance during electrochemical test, and the film can protect the weld metal from corrosion. In addition, the value of N in the fitting data reflects the roughness of the electrode surface and the uniformity of the corrosion current density distribution. The value of N is close to 1, the electrode surface is smooth and the corrosion current distribution is more uniform [27-30]. It can be seen from the fitting data that the corrosion product formed on the surfaces of the weld metal sample are relatively smooth under different heat input. After the weld metal samples are immersed in 3.5% NaCl solution for 5 days, the corrosion rates of the weld metal decrease and the corrosion property is improved due to the formation of a dense and smooth film on the surface of samples.

Compared with the corrosion current of the weld metal in Table 5 and Table 6, after the samples are immersed in 3.5wt% NaCl solution for 11 days, the corrosion current measured by the electrochemical test increases, and  $R_f$  and N of the corrosion product decrease, as presented in Table 7. When the heat input is  $10.7 \text{kJ} \cdot \text{cm}^{-1}$ ,  $I_{corr}$  of the weld metal is  $20.45 \mu\text{A} \cdot \text{cm}^{-2}$ , and it is nearly 4 times higher compared with the data in Table 6. The N value is far away from 1, it demonstrated that the surface roughness of the electrode increases, the actual capacitor deviates from the ideal (smooth) pure capacitor, and the corrosion product film appears looser [31,32].





**Figure 6.** Electrochemical corrosion behavior of the weld under different heat input  $9.2 \text{ kJ} \cdot \text{cm}^{-1}$ ,  $10.7 \text{ kJ} \cdot \text{cm}^{-1}$ ,  $11.9 \text{ kJ} \cdot \text{cm}^{-1}$ ,  $13.0 \text{ kJ} \cdot \text{cm}^{-1}$ ,  $14.4 \text{ kJ} \cdot \text{cm}^{-1}$  and  $15.9 \text{ kJ} \cdot \text{cm}^{-1}$  in 3.5% NaCl solution for 5 days (a: Potential polarization curve and b: EIS)



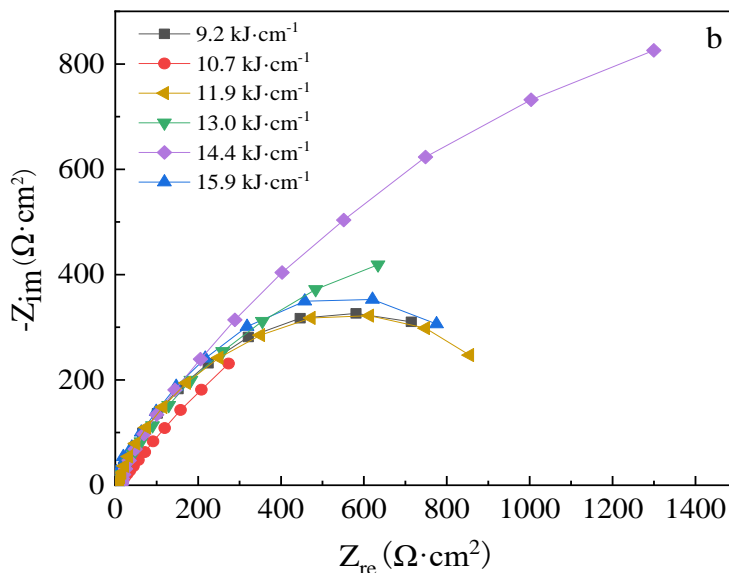


**Figure 7.** Electrochemical corrosion behavior of the weld under different heat input 9.2 kJ ·cm<sup>-1</sup>, 10.7 kJ ·cm<sup>-1</sup>, 11.9 kJ ·cm<sup>-1</sup>, 13.0 kJ ·cm<sup>-1</sup>, 14.4 kJ ·cm<sup>-1</sup> and 15.9 kJ ·cm<sup>-1</sup> in 3.5% NaCl solution for 11 days (a: Potential polarization curve and b: EIS)

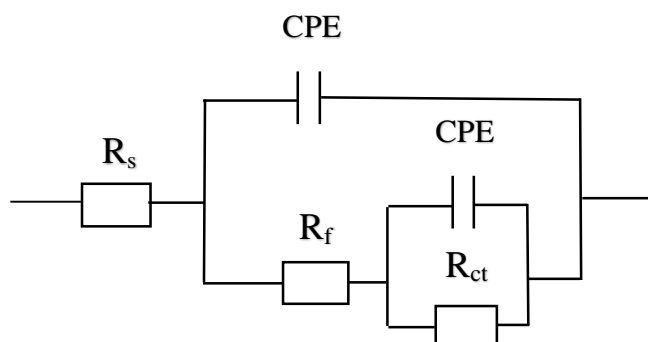


**Figure 8.** Equivalent circuit diagram for fitting impedance spectrum data in 3.5wt% NaCl solution for 5 days and 11 days

**Table 6.** Electrochemical test parameters of the weld metal at different heat input in a 3.5wt% NaCl solution for 5 days

Heat input (kJ·cm <sup>-1</sup> )	E <sub>corr</sub> (mV)	I <sub>corr</sub> (μA·cm <sup>-2</sup> )	R <sub>s</sub> (Ω·cm <sup>2</sup> )	CPE (F·cm <sup>-2</sup> )	R <sub>f</sub> (Ω·cm <sup>2</sup> )	R <sub>ct</sub> (Ω·cm <sup>2</sup> )	N
9.2	-723	9.84	18.82	0.001224	0.03456	1017	0.7982
10.7	-804	5.08	17.60	0.003488	1499	3061	0.7598
11.9	-775	7.04	19.03	0.001109	0.5602	998	0.6492
13.0	-735	4.23	15.94	0.005467	108.5	1839	0.6250
14.4	-770	4.59	12.65	0.001869	853.3	1436	0.7225
15.9	-773	8.23	13.65	0.002760	0.1	1055	0.8252

**Table 7.** Electrochemical test parameters of the weld metal at different heat input in a 3.5wt% NaCl solution for 11 days

Heat input (kJ·cm <sup>-1</sup> )	E <sub>corr</sub> (mV)	I <sub>corr</sub> (μA·cm <sup>-2</sup> )	R <sub>s</sub> (Ω·cm <sup>2</sup> )	CPE (F·cm <sup>-2</sup> )	R <sub>f</sub> (Ω·cm <sup>2</sup> )	R <sub>ct</sub> (Ω·cm <sup>2</sup> )	N
9.2	-739	9.98	4.43	0.003340	0.1	1114	0.6128
10.7	-848	20.45	6.43	0.010760	0.1858	950	0.4815
11.9	-765	17.91	5.93	0.002958	0.5324	1169	0.5493
13.0	-794	12.56	6.52	0.004308	0.01	1780	0.5772
14.4	-776	11.59	5.22	0.001959	100	3888	0.5371
15.9	-734	10.81	7.15	0.0019910	0.01	1516	0.5959

## 4. DISCUSSION

### 4.1 Corrosion behavior of weld metal in 3.5wt% NaCl solution

After the weld metal is immersed in 3.5% NaCl solution for different times, the corrosion products are formed on the surface of samples, and the samples with corrosion products are subjected to electrochemical test. After the samples are immersed in 3.5wt% NaCl solution for 5 days, a dense corrosion product film is formed on the surface of sample, and the film acts as an electrode to participate in electrochemical reaction. To a certain extent, the film can slow down corrosion rate of the weld metal and protect the weld metal from corrosion. On the contrary, after the samples are immersed in 3.5% NaCl solution for 11 days, the thickness of the corrosion product film formed on the surface of sample increases, due to the different density of different corrosion products, internal stress can occur to form crack defects inside the film, which result in the corrosion product film becoming loose and porous [33-35]. When the corrosion solution penetrates into the weld metal surface through defects, it can form a film/steel corrosion cell to accelerate the corrosion rate of the weld metal[36].

### 4.2 Effects of microstructure on the weld metal

The microstructure of the weld metal is composed of PF, FSP and AF. With the change of heat input, the amount of AF in the weld can also be different. When the heat input is 10.7kJ·cm<sup>-1</sup> and 11.9kJ·cm<sup>-1</sup>, the proportion of AF in the weld reaches the highest. The increase in the proportion of AF in weld can cause the corrosion property of the weld metal to decrease. This phenomenon is related to the characteristics of AF, the formation process of AF can be explained by diffusion and shear mechanisms [37,38]. During the transformation of AF, a large number of dislocations generate, resulting in the formation of polygonal ferrite with high dislocation density, more corrosion defects formation on the sample surface can accelerate the corrosion rate [39]. In addition, AF can increase the area of the grain boundary in the crystal, when the growth process of AF is completed, carbon can diffuse to the grain boundary, thereby carbon-rich film formation at the grain boundary can improve the activity of the

grain boundary [40,41]. Corrosion cell are formed between AF and other microstructures in 3.5wt% NaCl solution, and the galvanic effect can accelerate electrochemical corrosion rate of the weld metal. Thus, the change of corrosion rate is related to the change of microstructure.

## 5. CONCLUSION

Based on microstructure observation, the weight loss tests, potentiodynamic polarization and EIS tests, it is concluded that the corrosion behavior of the weld metal is affected by microstructure and corrosion products. With the change of heat input, the amount of AF in the weld metal shows unequal. When the heat input is  $11.9\text{kJ} \cdot \text{cm}^{-1}$ , the amount of AF is 89.24%, the corrosion current density reaches the maximum value and the corrosion rate is the fastest. Therefore, the amount of AF in the weld can effect on corrosion property of the weld metal in 3.5wt% NaCl solution. In addition, the thickness and density of the corrosion products on the surface of the weld metal play an important role in corrosion behavior of the weld metal. After the samples are immersed in 3.5wt% NaCl solution for 5 days, the corrosion product film can protect the weld metal from corrosion to slow down the corrosion rate of the weld metal. As the samples are immersed in 3.5wt% NaCl solution for 11 days, the corrosion product film thickness increases and the corrosion product film becomes looser, which promotes the corrosion rate of the weld metal.

## ACKNOWLEDGEMENTS

The present research is financially supported by the Science and Technology Research Project of Department of Education of Liaoning Province (No. L2017LQN021).

## References

1. A. K. Padap, G. P. Chaudhari, V. Pancholi and S. K. Nath, *J. Mater. Sci.*, 47(2012) 7894.
2. H. Dai, X. Yan and H. Jiang, *Int. J. Mech. Mater. Des.*, 10(2014) 411.
3. N. Prasad, S. Kumar, P. Kumar and S. N. Ojha, *J. Mater. Sci.*, 26(1991) 5158.
4. H. Dai, X. Yan and T. Dai, *Int. J. Mech. Mater. Des.*, 11(2015) 221.
5. Z. Wang, J. Wu, J. Li, X. Wu, Y. Huang and X. Li, *Metall. Mater. Trans. A*, 49(2018) 187.
6. M. Nouredine and O. Allaoui, *Int. J. Adv. Manuf. Technol.*, 106(2020) 2689.
7. Y. Shi, Z. Han and J. Fu, *Int. J. Fracture*, 91(1998) 349.
8. C. Liu, L. Shi, Y. Liu, C. Li, H. Li and Q. Guo, *J. Mater. Sci.*, 51(2016) 3555.
9. R. A. Ricks, P. R. Howell and G. S. Barritte, *J. Mater. Sci.*, 17(1982) 732.
10. H. Dong, X. Hao and Dewei Deng, *Metallogr. Mstrc. Anls.*, 3(2014) 138.
11. K. Prasad and D. K. Dwivedi, *Int. J. Adv. Manuf. Tech.*, 36(2008) 475.
12. H. Zhao, B. P. Wynne and E. J. Palmiere, *J. Mater. Sci.*, 53(2018) 3785.
13. S. K. Dhua, D. Mukerjee and D. S. Sarma, *Metall. Mater. Trans. A*, 34(2003) 241.
14. C. Ren, X. Zhang, H. Ji, Z. Nan and Z. Qiao, *Mater. Sci. Eng. A*, 705(2017) 394.
15. A. F. Gourgues, H. M. Flower and T.C. Lindley, *Mater. Sci. Tech.*, 16(2000) 26.
16. J. M. Rodriguez-Ibabe, I. Gutiérrez and B. López, *Mater. Sci. Forum*, 284-286(1998) 419.
17. B. Liao and F. R. Xiao, *Trans. Mater. Heat Treat.*, 30(2009) 57.

18. Y. M. Kim, H. Lee and Nack J. Kim, *Mater. Sci. Eng. A*, 478(2008) 361.
19. M. C. Zhao, F. R. Xiao, Y. Y. Shan, Y. H. Li and K Yang, *Acta Metall. Sin.*, 38 (2002) 283.
20. J. S. Byun, J. H. Shim, J.Y. Suh, Y. J. Oh, Y. W, Cho, J. D. Shim and D. N. Lee, *Mater. Sci. Eng. A*, 319–321(2001) 326.
21. Y. M. Kim, H. Lee and Nack J.Kim, *Mater. Sci. Eng. A*, 478(2008) 361.
22. D. Zhang, H. Terasaki and Y. Komizo, *Acta Mater.*, 58(2010) 1369.
23. M. M. Hosseinioun and G. Moeini, *Mater. Test.*, 58(2016) 848.
24. W. Liu, Y. Zhang, H. Zhang, Z. Qu and Jinfu Li, *J. Solid State Electrochem.*, 13(2009) 1645.
25. F. Ma, Y. Zhang, H. Wang, W. Li and B. Hou, *Int. J. Electrochem. Sci.*, 13(2018) 235.
26. Y. Guo, C. Li, Y. Liu, L. Yu, Z. Ma, C. Liu and Hui-jun Li, *Int. J. Miner. Metall. Mater.*, 22(2015) 604.
27. D. Loder, S. K. Michelic, A. Mayerhofer and Christian Bernhard, *Metall. Mater. Trans. B*, 48(2017) 1992.
28. S. Wang, Y. Zuo, Y. Tang and X. Zhao, *Int. J. Electrochem. Sci.*, 13(2018) 842.
29. Y. Lu, H. Jing, Y. Han and L. Xu, *J. Mater. Eng. Perform.*, 25(2016) 565.
30. H. Wang, P. Zhou, S. Huang and C. Yu, *Int. J. Electrochem. Sci.*, 11(2016) 1293.
31. M. P. Garcia, G. L. Mantovani, R. V. Kumar and Renato Altobelli Antunes, *J. Mater. Eng. Perform.*, 26(2017) 4718.
32. R. R. Mahato, A.K. Bhattamishra, R. Singh and P. Jayakrishnan, *Anti-Corros. Method. M.*, 48(2001) 188.
33. D. Zhou, J. Wang, Y. Gao, L. Zhang, *Int. J. Electrochem. Sci.*, 12(2017) 192.
34. I. G. Rodionova, A. V. Amezhnov, D. L. D'yakonov, N. G. Shaposhnikov, O. N. Baklanova and Y. S. Gladchenkova, *Metall.*, 63(2020) 1165.
35. S. J. Oh, D.C. Cook and H.E. Townsend, *Hyperfine Interac.*, 112(1998) 59.
36. D. Zhou, J. Wang, Z. Han, X. Liu and J. Mao, *Int. J. Electrochem. Sci.*, 12(2017) 639.
37. H. Ji, Y. Chen and Sh. Chen, *Adv. Mater. Res.*, 557-559(2012) 143.
38. W. Liu, Q. Zhou, L. Li, Z. Wu and Zhifang Gao, *J. Alloys Comp.*, 598(2014) 198.
39. F. F. Eliyan, E. S. Mahdi and A. Alfantazi, *Int. J. Electrochem. Sci.*, 8(2013) 578.
40. M. A. Ameer, A. M. Fekry and S. M. Shanab, *Int. J. Electrochem. Sci.*, 6(2011) 1572.
41. E.F. Diaz, J.G. Gonzalez-Rodriguez, R. Sandoval-Jabalera, S. Serna, B. Campillo, M. A. NeriFlores, C. GaonaTiburcio and A. Martinez-Villafañe, *Int. J. Electrochem. Sci.*, 5(2010) 578.